Reduced tyrosine kinase inhibitor dose is predicted to be as effective as standard dose in chronic myeloid leukemia: a simulation study based on phase III trial data

Artur C. Fassoni,[1,2] Christoph Baldow,[2] Ingo Roeder[2,3]* and Ingmar Glauche[2]*

[1]Instituto de Matemática e Computação, Universidade Federal de Itajubá, Brazil; [2]Institute for Medical Informatics and Biometry, Faculty of Medicine Carl Gustav Carus, Technische Universität Dresden, Germany and [3]National Center for Tumor Diseases (NCT), Partner Site Dresden, Germany

**IR and IG contributed equally to this work.*

©2018 Ferrata Storti Foundation. This is an open-access paper. doi:10.3324/haematol.2018.194522

Received: March 29, 2018.

Accepted: June 26, 2018.

Pre-published: June 28, 2018.

Correspondence: ingmar.glauche@tu-dresden.de

Reduced tyrosine kinase inhibitor dose is predicted to be as effective as standard dose in chronic myeloid leukemia: A simulation study based on phase 3 trial data.

Artur Fassoni[1,2] , Christoph Baldow[2] , Ingo Roeder[2,3] , Ingmar Glauche[2]

[1]Instituto de Matemática e Computação, Universidade Federal de Itajubá, Itajubá, Brasil

[2]Institute for Medical Informatics and Biometry, Faculty of Medicine Carl Gustav Carus, Technische Universität Dresden, Dresden, Germany

[3]National Center for Tumor Diseases (NCT), Partner Site Dresden, Dresden, Germany

Supplementary material

Content

Online Supplementary Texts

S1 Model setup

The total number of proliferating stem cells is set to $T_Y = 10^6$ cells [1]. The total numbers of quiescent stem cells and differentiated cells are assumed to satisfy steady-state conditions within our model equations, which leads to $T_X = (p_{YX}/p_{XY})T_Y$ and $T_W = (p_W/r_W)T_Y$. To describe a number of differentiated cells much higher than the number of proliferating stem cells, we define the total number of differentiated cells by $T_W = 10^{12}$ [1], thereby implying that parameters p_W and r_W shall satisfy the relation $p_W/r_W = 10^6$. Assuming that the mean lifetime $1/r_W$ of a differentiated cell is about 7.5 days [2], i.e., 0.25 months, we have $r_W = 4$ month^{-1}, and $p_W = 4 \times 10^6$ cells/month, which can be interpreted as the monthly production of differentiated leukemic cells by each proliferating stem cell.

The modeled *BCR-ABL1* levels in each cell compartment, L^X_{MOD}, L^Y_{MOD} and L^W_{MOD}, are described as the proportion of leukemic cells in each compartment, i.e.,

$$L^X_{MOD}(t) = 100 \times \frac{Y(t)}{T_X}, \quad L^Y_{MOD}(t) = 100 \times \frac{Y(t)}{T_Y}, \quad L^W_{MOD}(t) = 100 \times \frac{W(t)}{T_W}. \tag{SE1}$$

These are the mathematical expressions used to calculate the *BCR-ABL1* levels shown in the Figures of our manuscript. We point out that a potential constant bias in the correspondence between *BCR-ABL1* levels and tumor load does not change the results of our analysis, since it only affects the intercepts A and B of the biexponential fit, while the slopes α and β remain the same (see also Online Supplementary Text S2).

The initial conditions assume that the initial *BCR-ABL1* level in each compartment is equal to the observed initial *BCR-ABL1* L_0 level of each patient,

$$Y(0) = Y_0 = \frac{L_0}{100} T_Y, \quad X(0) = \frac{L_0}{100} T_X = \frac{p_{YX}}{p_{XY}} Y_0, \quad W(0) = \frac{L_0}{100} T_W = \frac{p_w}{r_W} Y_0.$$

Competition between normal and leukemic cells is described implicitly, through the assumption of constant total cell numbers in each cell compartment. This assumption of constant total cell numbers (normal+leukemic) reflects the idea of a competition for limited resources and niche space. Therefore, during therapy, each leukemic cell removed by the TKI effect is replaced by a normal cell in the corresponding compartment. Off therapy, the population of leukemic cells expands and outcompetes their normal counterparts; for each new leukemic cell, a normal cell is removed. It is important to note that, off-therapy, as the number of leukemic cells grows, the total number of cells may eventually surpass the levels described by T_Y, T_X and T_W. This is an aspect which is also well known for late chronic and accelerated phases of CML which are characterized by high cell counts. Technically, the assumption of a constant cell number is a simplification of a more complex, potentially regulated process. Our results do not depend on the precise choice of a fixed compartment size.

S2 Model solution and correspondence between phenomenological and mechanistic parameters

In our differential equation model, the first two equations form a decoupled linear system, which can be written in vector form as

$$\frac{d}{dt} \begin{bmatrix} X \\ Y \end{bmatrix} = \begin{bmatrix} p_{XY} & -p_{YX} - q \\ -p_{XY} & p_{YX} \end{bmatrix} \begin{bmatrix} X \\ Y \end{bmatrix}. \tag{SE2}$$

Using standard methods for solving linear systems of ODEs, we obtain the solutions

$$Y(t) = Y_0 \left(C_1 e^{\lambda_1 t} + C_2 e^{\lambda_2 t} \right) \text{ and } X(t) = Y_0 \left(C_3 e^{\lambda_1 t} + C_4 e^{\lambda_2 t} \right), \tag{SE3}$$

where λ_1 and λ_2 are the eigenvalues of the linear system (SE2),

$$\lambda_1 = \frac{1}{2} \left(-p_{XY} - p_{YX} - q - \sqrt{(p_{XY} + p_{YX} + q)^2 - 4 p_{XY} q} \right), \; \lambda_2 = \frac{1}{2} \left(-p_{XY} - p_{YX} - q + \sqrt{(p_{XY} + p_{YX} + q)^2 - 4 p_{XY} q} \right).$$

and the constants C_1, C_2, C_3 and C_4 are

$$\begin{aligned}
C_1 &= \frac{-p_{XY}-p_{YX}+q+\sqrt{(p_{XY}+p_{YX}+q)^2-4p_{XY}q}}{2\sqrt{(p_{XY}+p_{YX}+q)^2-4p_{XY}q}},\\
C_2 &= \frac{p_{XY}+p_{YX}-q+\sqrt{(p_{XY}+p_{YX}+q)^2-4p_{XY}q}}{2\sqrt{(p_{XY}+p_{YX}+q)^2-4p_{XY}q}},\\
C_3 &= \frac{p_{YX}}{p_{XY}}\left(\frac{-p_{XY}-p_{YX}-q+\sqrt{(p_{XY}+p_{YX}+q)^2-4p_{XY}q}}{2\sqrt{(p_{XY}+p_{YX}+q)^2-4p_{XY}q}}\right),\\
C_4 &= \frac{p_{YX}}{p_{XY}}\left(\frac{p_{XY}+p_{YX}+q+\sqrt{(p_{XY}+p_{YX}+q)^2-4p_{XY}q}}{2\sqrt{(p_{XY}+p_{YX}+q)^2-4p_{XY}q}}\right).
\end{aligned} \tag{SE4}$$

Substituting the expression of solution $Y(t)$ in the expression of $L^Y_{MOD}(t) = 100 \times (Y(t)/T_Y)$ and using the definition of Y_0, the *modeled BCR-ABL1* levels of proliferating LSCs can be written as

$$L^Y_{MOD}(t) = K_1 e^{\lambda_1 t} + K_2 e^{\lambda_2 t},$$

where $K_i = L_0\, C_i$, for $i = 1,2$.

On the other hand, the *observed BCR-ABL1* levels are described by **the phenomenological characteristics as (in terms of A, B, α and β, see main text)**

$$L_{OBS}(t) = Ae^{\alpha t} + Be^{\beta t}.$$

The structural similarity between the modeled *BCR-ABL1* ratio, $L^Y_{MOD}(t)$, and the observed biphasic decline, $L_{OBS}(t)$, allows to express the phenomenological (i.e., clinically observable) parameters (A, B, α, β) in terms of the mechanistic (i.e., functionally interpretable) parameters (p_{XY}, p_{YX}, q, L_0), and vice-versa. Indeed, we can equal the expressions of $L^Y_{MOD}(t)$ and $L_{OBS}(t)$ and obtain:

$$\begin{aligned}
\alpha = \lambda_1 &= \frac{1}{2}\left(-p_{XY}-p_{YX}-q-\sqrt{(p_{XY}+p_{YX}+q)^2-4p_{XY}q}\right),\\
\beta = \lambda_2 &= \frac{1}{2}\left(-p_{XY}-p_{YX}-q+\sqrt{(p_{XY}+p_{YX}+q)^2-4p_{XY}q}\right),\\
A = K_1 &= L_0\frac{\left(-p_{XY}-p_{YX}+q+\sqrt{(p_{XY}+p_{YX}+q)^2-4p_{XY}q}\right)}{2\sqrt{(p_{XY}+p_{YX}+q)^2-4p_{XY}q}},\\
B = K_2 &= L_0\frac{\left(p_{XY}+p_{YX}-q+\sqrt{(p_{XY}+p_{YX}+q)^2-4p_{XY}q}\right)}{2\sqrt{(p_{XY}+p_{YX}+q)^2-4p_{XY}q}}.
\end{aligned} \tag{SE5}$$

Inverting these formulas, we have

$$L_0 = A+B, \quad q = -\frac{\alpha A+\beta B}{A+B}, \quad p_{XY} = -\frac{\alpha\beta(A+B)}{\alpha A+\beta B}, \quad p_{YX} = -\frac{AB(\alpha-\beta)^2}{(A+B)(\alpha A+\beta B)}. \tag{SE6}$$

We denote this correspondence between the phenomenological and mechanistic parameters as the exact solution. With the above correspondences, we derive an explicit determination of model parameters based on the kinetic parameters estimated from the patient data. In fact, for each patient the individual values of A, B, α and β are calculated by fitting a bi-exponential regression model to the *BCR-ABL1* levels of individual patients. From these estimates, the individual values of L_0, q, p_{XY} and p_{YX} are calculated with equations (SE6). Using these values, the model simulations reproduce the bi-exponential fit of the patient specific *BCR-ABL1* levels. See Online Supplementary Figure S1 for the time courses of each of the 122 selected patients.

S3 Model parameters values

Using the above correspondence, the median parameter values obtained from the available dataset of 122 selected patients were $q = 1.00394$, $p_{XY} = 0.05380$, $p_{YX} = 0.00095$ and $L_0 = 106.6\%$. Using these values and the median latency time of $T = 6.88$ years, we estimated a median value of the proliferation rate $p_Y = 0.18701$. In all figures illustrating the model behavior (figures 1C, 2, 3; Online Supplementary Figures S2, S3, S4, S5, S6, S8, S9, S10), we used approximated median

values, given by $q = 1$, $p_{XY} = 0.05$, $p_{YX} = 0.001$, $L_0 = 100\%$ and $p_Y = 0.2$ (corresponding to a latency time $T = 6.45$ years). In figure 4C, we used the values $q = 0.9$, $p_{XY} = 0.055$, $p_{YX} = 0.004$, $L_0 = 100\%$ and $p_Y = 0.24$.

In the Online Supplementary Text S13 we show that an alternative model formulation without LSCs deactivation ($p_{YX} = 0$) leads to qualitatively similar results.

S4 Stochastic model simulations

The critical events, which determine the efficacy of low-dose TKI, occur when *BCR-ABL1* ratios are low and proliferating LSCs are present in the hundreds (Online Supplementary Figure S2). Stochastic effects could generate different results regarding treatment failure, due to changes in the time to rebound of proliferating LSCs. Therefore, we implemented a stochastic version of the ODE model using a Gillespie algorithm. The stochastic transitions considered were:

$$X \xrightarrow{p_{XY}} Y,\ Y \xrightarrow{p_{YX}} X,\ Y \xrightarrow{p_Y} 2Y,\ Y \xrightarrow{e_{TKI}} \emptyset,\ Y \xrightarrow{p_W} Y + W,\ W \xrightarrow{r_W} \emptyset.$$

We've used the same model parameters as in the illustrative figures showing the ODE simulations: $p_Y = 0.2$, $e_{TKI} = q + p_Y = 1.2$, $p_{XY} = 0.05$, $p_{YX} = 0.001$, $L_0 = 100\%$, $r_W = 4$ and $p_W = 4 \times 10^6$. We simulated the stochastic model 1,000 times. The results of several representative stochastic simulations (Online Supplementary Figure S11) show that the overall dynamics are the same, thereby largely excluding different outcomes and implying that even in the stochastic scenario the TKI dose reduction is expected to retain the long-term treatment efficiency.

S5 Approximations for slopes α and β

The exact solution can be simplified by scaling arguments. Indeed, the distributions of parameters q, p_{XY} and p_{YX} in the patient population show that these parameters are dispersed over several orders of magnitude (figure 1B). Therefore, defining the scaling parameters

$$\varepsilon_1 = \frac{p_{YX}}{p_{XY}},\ \varepsilon_2 = \frac{p_{XY}}{q},\ \varepsilon_3 = \frac{p_{YX}}{q} = \varepsilon_1\varepsilon_2,$$

we can derive simplified expressions for the slopes α and β. To simplify the expression for $\alpha = \lambda_1$, we substitute $p_{YX} = \varepsilon_1\varepsilon_2 q$ and $p_{XY} = \varepsilon_2 q$ in (SE5) and obtain

$$\alpha = \lambda_1 = -q\left(\frac{1 + \varepsilon_2 + \varepsilon_1\varepsilon_2 + \sqrt{(1 + (1+\varepsilon_1)\varepsilon_2)^2 - 4\varepsilon_2}}{2}\right).$$

Expanding this expression in power series of ε_2 we have

$$\alpha = \lambda_1 = -q\left(1 + \varepsilon_1\varepsilon_2 + \varepsilon_1 O(\varepsilon_2^2)\right) = -q\left(1 + O(\varepsilon_3)\right).$$

Similarly, to simplify the expression of $\beta = \lambda_2$, we substitute $p_{YX} = \varepsilon_1 p_{XY}$ and $q = p_{XY}/\varepsilon_2$ in (SE5), and expand the result in a power series of ε_2. We obtain

$$\beta = \lambda_2 = -p_{XY}\left(1 - \varepsilon_1\varepsilon_2 + \varepsilon_1 O(\varepsilon_2^2)\right) = -p_{XY}\left(1 + O(\varepsilon_3)\right).$$

Due to the negligible magnitude of ε_3, we can approximate the slopes as $\alpha \approx \alpha^* = -q$, and $\beta \approx \beta^* = -p_{XY}$.

This is referred to as the approximated solution. Due to the very good agreement between exact and approximated solutions (relative error of 0.1% for the median patient) and the simplicity of the approximated formulas, one can directly interpret the bi-phasic decline in terms of the underlying mechanisms (figure 1C,D, Online Supplementary Figure S2).

S6 Approximations for model solutions

Additionally, we deduce approximations $Y^*(t)$ and $X^*(t)$ for the numbers of proliferating and quiescent LSCs, as well approximations $L^{Y*}_{MOD}(t)$ and $L^{X*}_{MOD}(t)$ for the respective modeled *BCR-ABL1* levels. See figure 1C and Online Supplementary Figure S2 for a comparison of such approximations with exact solutions.

First, substituting $p_{YX} = \varepsilon_1\varepsilon_2 q$ and $p_{XY} = \varepsilon_2 q$ in the expressions for C_1 and C_2, and expanding the results as power series of ε_2, we obtain

$$C_1 = 1 - \varepsilon_3 + O(\varepsilon_2\varepsilon_3) \text{ and } C_2 = \varepsilon_3 + O(\varepsilon_2\varepsilon_3).$$

Retaining the terms up to order ε_3, we obtain the approximations

$$C_1 \approx C_1^* = 1 - \frac{p_{YX}}{q} \text{ and } C_2 \approx C_2^* = \frac{p_{YX}}{q}. \tag{SE7}$$

Additionally, using the approximations $\lambda_1 = \alpha \approx -q$ and $\lambda_2 = \beta \approx -p_{XY}$, we obtain the approximation

$$Y(t) \approx Y^*(t) = Y_0\left(C_1^* e^{qt} + C_2^* e^{-p_{XY}t}\right) = Y_0\left(1 - \frac{p_{YX}}{q}\right)e^{-qt} + Y_0\left(\frac{p_{YX}}{q}\right)e^{-p_{XY}t}. \tag{SE8}$$

The corresponding approximation for the *BCR-ABL1* levels of proliferating LSCs is

$$L^Y_{MOD}(t) \approx L^{Y*}_{MOD}(t) = 100 \times \frac{Y^*(t)}{T_Y} = L_0\left(1 - \frac{p_{XY}}{q}\right)e^{-qt} + L_0\frac{p_{XY}}{q}e^{-p_{XY}t}. \tag{SE9}$$

Now, we obtain approximations for the quiescent LSCs. To simplify the expressions for C_3 and C_4, we use the same procedure as above for C_1 and C_2, and obtain

$$C_3 = -\varepsilon_3 - \varepsilon_2\varepsilon_3 + O(\varepsilon_3\varepsilon_2^2), \quad C_4 = \varepsilon_1 + \varepsilon_3 - \varepsilon_2\varepsilon_3 + O(\varepsilon_3\varepsilon_2^2 + \varepsilon_3^2).$$

Taking approximations of order ε_3 and using the definitions of ε_1 and ε_3, we obtain

$$C_3 \approx C_3^* = -\frac{p_{YX}}{q}, \quad C_4 \approx C_4^* = \frac{p_{YX}}{p_{XY}} + \frac{p_{YX}}{q}.$$

Therefore, the exact solution $X(t)$ in (SE3) is approximated by

$$X(t) \approx Y_0\left(C_3^* e^{\lambda_1^* t} + C_4^* e^{\lambda_2^* t}\right) = -Y_0\frac{p_{YX}}{q}e^{-qt} + Y_0\left(\frac{p_{YX}}{p_{XY}} + \frac{p_{YX}}{q}\right)e^{-p_{XY}t}.$$

At a first look, this expression indicates that the quiescent LSCs also show a bi-exponential decline. Although this is true, the effect of the first decline is negligible. To see this, note that the last expression can be written as

$$X(t) \approx Y_0\,\frac{p_{YX}}{p_{XY}}\left(e^{-p_{XY}t} + \varepsilon_2(e^{-p_{XY}t} - e^{-qt})\right).$$

From this expression we see that the first decline is sensed only at order ε_2, and it is also balanced with a slower decline $e^{-p_{XY}t}$ at the same order. Therefore, the leading order approximation (with respect to ε_2) already provides a good approximation, and we consider the approximation

$$X(t) \approx X^*(t) = Y_0\,\frac{p_{YX}}{p_{XY}}e^{-p_{XY}t}. \tag{SE10}$$

The corresponding approximation for the *BCR-ABL1* levels of quiescent LSCs is

$$L^X_{MOD}(t) \approx L^{X*}_{MOD}(t) = 100 \times \frac{X^*(t)}{T_X} = L_0 e^{-p_{XY}t}. \tag{SE11}$$

S7 Relationship between the numbers of quiescent and proliferating LSCs after the second decline

From equations (SE8) and (SE10), we see that, after the first decline (i.e., for $e^{-qt} \approx 0$), the numbers of quiescent and proliferating LSCs are approximated by

$$X(t) \approx Y_0\frac{p_{YX}}{p_{XY}}e^{-p_{XY}t} \text{ and } Y(t) \approx= Y_0\frac{p_{YX}}{q}e^{-p_{XY}t}.$$

Thus, the ratio $X(t)/Y(t)$ after the first decline is given approximately by $X(t)/Y(t) \approx q/p_{XY}$. Since $\alpha \approx -q$ and $\beta \approx -p_{XY}$, we can approximate the fraction q/p_{XY} by α/β and also write the following approximation for t after the first decline, $X(t)/Y(t) \approx \alpha/\beta$. Therefore, after the first decline the proportion quiescent/proliferating LSCs is equal to $q/p_{XY} \approx \alpha/\beta$ and remains constant in the long-term.

S8 Threshold for optimal favorable reduction of TKI dose

In this section, we deduce an expression for the optimal favorable reduction fraction f_{OPT}, equation (E5) in the Main Text. We seek for a fraction of the standard dose which separates two types of behavior of the long-term treatment efficiency, $|\beta|$, as shown in figure 2A and Online Supplementary Figure S3: for doses above f_{OPT}, $|\beta|$ is roughly constant, near the original long-term treatment efficiency (green region in figure 2A), while for doses below f_{OPT}, the value of $|\beta|$ decreases fast as the dose is reduced (red region in figure 2A).

We start by substituting $p_{YX} = \varepsilon_1 p_{XY}$ in the expression for β in (SE5), and expanding the result as power series of ε_1, obtaining

$$\beta = -p_{XY}\left(1 - \varepsilon_1\frac{p_{XY}}{q - p_{XY}} + \varepsilon_1^2\frac{q p_{XY}^2}{(q - p_{XY})^3} + O(\varepsilon_1^3)\right).$$

The relative difference between the activation rate of quiescent LSCs, p_{XY}, and the actual long-term treatment efficiency $|\beta|$ is

$$\frac{p_{XY}-|\beta|}{p_{XY}} = \varepsilon_1 \frac{p_{XY}}{q-p_{XY}} + O(\varepsilon_1^2). \tag{SE12}$$

For all patients within our data-set, the individual parameters satisfy $q > p_{XY}$, indicating that the net effect of TKI, cell removal minus LSCs proliferation, $q = e_{TKI} - p_Y$, is always larger than quiescent LSC activation, p_{XY}. Therefore, the relative difference in (SE12) is always positive, implicating that the maximally achievable long-term treatment efficiency $|\beta|$ equals p_{XY}. For the original dose, the actual long-term treatment efficiency is already very near this maximum value. Indeed, for the median patient in our data-set, (SE12) corresponds to a relative difference of only 1.6% with respect to the maximum value. Therefore, an increase in the dose does not lead to a relevant increase in the long-term treatment efficiency (Online Supplementary Figure S3). On the other hand, we seek for an optimal reduction in the dose for which the new treatment efficiency is still very near the maximum p_{XY}.

We first note that the relative difference (SE12) changes as the TKI dose changes. Indeed, substituting $q = e_{TKI} - p_Y$, (SE12) rewrites as

$$\frac{p_{XY}-|\beta|}{p_{XY}} = \varepsilon_1 \frac{p_{XY}}{e_{TKI}-p_Y-p_{XY}} + O(\varepsilon_1^2). \tag{SE13}$$

Assuming a linear dose-response relationship (see section 9 "Pharmacokinetic modeling, model simplification, and relationship between TKI-effect and TKI-dose" for a justification on the plausibility of such hypothesis), the TKI effect e_{TKI} is reduced to a fraction $f \cdot e_{TKI}$, when the dose is reduced by a fraction f. Therefore, the dependence of the relative difference (SE13) as a function of the dose fraction f is written as

$$\frac{p_{XY}-|\beta|}{p_{XY}} = \varepsilon_1 \frac{p_{XY}}{f\cdot e_{TKI}-p_Y-p_{XY}} + O(\varepsilon_1^2). \tag{SE14}$$

We focus on the first-order relative difference, i.e.,

$$\frac{p_{XY}-|\beta|}{p_{XY}} \approx \varepsilon_1 u(f),$$

where

$$u(f) = \frac{p_{XY}}{f\cdot e_{TKI}-p_Y-p_{XY}},$$

As the dose is reduced, the value of f decreases, and the denominator of $u(f)$ decreases. This leads to an increase in $u(f)$ and, therefore, an increase in the first-order relative difference. The derivative of the function $u(f)$ satisfies $u'(f) = -(e_{TKI}/p_{XY})(u(f))^2$. This relation implies that the rate of change in u is proportional to its square u^2. Thus, the condition $u(f) = 1$ defines the threshold between a region of slow change in u (when $u(f) < 1$), and a region of fast change in u (when $u(f) > 1$). Thus, when $u(f) > 1$, the function $u(f)$ increases very fast as f decreases, and diverges to $+\infty$ when the value of f makes the denominator approaching zero. Consequently, we define the optimal threshold in the dose reduction as the value f_{OPT} such that

$$u(f_{OPT}) = 1.$$

For this choice, the first order relative difference is

$$\frac{p_{XY}-|\beta|}{p_{XY}} \approx \varepsilon_1 u(f_{OPT}) = \varepsilon_1.$$

Solving $u(f_{OPT}) = 1$ for f_{OPT}, we find that the optimal reduction fraction is

$$f_{OPT} = \frac{p_Y + 2p_{XY}}{e_{TKI}}. \tag{SE15}$$

From our estimates it follows that the optimal reduced dose within the patient cohort of 122 selected patients leads to a minor decline in the treatment efficiency in the order of 3% (IQR [0.2%,8.8%]) (corresponding to $100\times\varepsilon_1$%), while the dose can potentially be reduced to 25% of the original dose (IQR [14%,39%]).

S9 Adaptive treatment optimization

Here, we present the deduction of formula (E6) in the Main Text, which expresses p_Y in terms of (α,β,A,B,B',f). First, from equations (SE5) and (SE7), the intercept B can be approximated as

$$B = K_2 = L_0 C_2 \approx \frac{p_{YX}}{q} L_0. \tag{SE16}$$

This approximation is valid for the standard dose as well as for the reduced dose. In the latter case, with the reduction of the dose to a fraction $f \in [0,1]$ of original dose, the new parameters are $e'_{TKI} = f e_{TKI}$ and $q' = e'_{TKI} - p_Y$, while the new intercept B' is

$$B' \approx \frac{p_{YX}}{q'} L_0. \tag{SE17}$$

Isolating $q = e_{TKI} - p_Y$ and $q' = f e_{TKI} - p_Y$ in (SE16) and (SE17), we obtain the system:

$$\begin{cases} e_{TKI} - p_Y \approx \dfrac{p_{XY}}{B} L_0, \\ \\ f e_{TKI} - p_Y \approx \dfrac{p_{XY}}{B'} L_0. \end{cases} \tag{SE18}$$

with unknown parameters p_Y and e_{TKI}. Indeed, for each patient, parameters B and $L_0 = A + B$ are observable from the biexponential fit, while p_{XY} can be calculated using (SE6). The new intercept B' is obtained from the response observed after a dose reduction to a fraction f of the original dose. Solving system (SE18) for p_Y and e_{TKI} we obtain

$$p_Y \approx \frac{p_{YX} L_0}{1-f} \left(\frac{f}{B} - \frac{1}{B'} \right) \quad \text{and} \quad e_{TKI} \approx \frac{p_{YX} L_0}{1-f} \left(\frac{1}{B} - \frac{1}{B'} \right).$$

Now, the values of p_Y and e_{TKI} can be used in expression (SE15) and the optimal dose reduction fraction f_{OPT} can be calculated for each individual patient.

For clinical applicability, we would like to have an expression depending only on the phenomenological parameters. Using approximations $B \approx (p_{YX}/q) L_0$ and $|\alpha| \approx q$, the expression for p_Y can be simplified as

$$p_Y \approx \frac{q}{1-f} \frac{p_{YX} L_0}{q} \left(\frac{f}{B} - \frac{1}{B'} \right) \approx \frac{|\alpha|\, B}{1-f} \left(\frac{f}{B} - \frac{1}{B'} \right). \tag{SE19}$$

The optimal reduction fraction f_{OPT} can also be expressed only in terms of the phenomenological parameters. Indeed, substituting the above expression for p_Y and approximations $|\alpha| \approx q$ and $|\beta| \approx p_{XY}$ in equation (SE15), we obtain

$$f_{OPT} = \frac{p_Y + 2p_{XY}}{p_Y + q} \approx \frac{\dfrac{B}{1-f} \left(\dfrac{f}{B} - \dfrac{1}{B'} \right) + 2 \left| \dfrac{\beta}{\alpha} \right|}{\dfrac{B}{1-f} \left(\dfrac{f}{B} - \dfrac{1}{B'} \right) + 1}. \tag{SE20}$$

S10 Pharmacokinetic modeling, model simplification, and relationship between TKI-effect and TKI-dose

In this section, we present an enhanced model of TKI treatment encompassing pharmacokinetic aspects, such as TKI daily intake and decay. Then, we compare this more complex model to the simplified model used throughout our paper (equations E2-E4), which considers a constant mean TKI concentration over the time. We show how the detailed model is an extension of the simplified model and demonstrate that the results of the simplified model agree with those of the enhanced model. Finally, we show that, under reasonable assumptions, a dose reduction by a fraction f is equivalent to a reduction in the TKI-effect e_{TKI} by the same fraction f.

We start considering the following extension of our ODE model, in which we explicitly consider the plasma concentration $I(t)$ of the TKI:

$$\begin{aligned} \frac{dX}{dt} &= -p_{XY} X + p_{YX} Y \\ \\ \frac{dY}{dt} &= p_{XY} X - p_{YX} Y + p_Y Y - k_{TKI} I Y \\ \\ \frac{dW}{dt} &= p_W Y - r_W W \\ \\ \frac{dI}{dt} &= v(t) - \tau I \end{aligned} \tag{SE21}$$

The cytotoxic effect of the TKI is described by the term $-k_{TKI} I Y$, for which we assume a linear drug-response relationship within a therapeutic window. This follows the mass action law, where a change in the abundance of TKI leads to a proportional change in the number of proliferating LSCs targeted by the TKI. This choice reflects the *log-kill hypothesis* or the *fractional cell kill hypothesis*, stating that a given fixed amount of drug (TKI) kills a fixed fraction of proliferating cells (LSCs), independent of the absolute number of cells.

The administration of TKI is modeled by the time-dependent function $v(t)$, and the TKI decay is described by the parameter τ, i.e., the half-life of the TKI is given by $T_{1/2} = \log(2)/\tau$. For both TKI *imatinib* and *dasatinib*, CML patients take one dose ν per day (for *imatinib*, the common daily dose is $\nu_{im} = 400$ mg; for *dasatinib*, the standard dose is $\nu_{da} = 100$ mg). This daily-dose scheduling can be described by

$$v(t) = \sum_{i=1}^{n_d} \nu\delta(t - t_i) \tag{SE22}$$

where $\delta(t - t_i)$ is the Dirac-Delta function, representing one single daily drug intake at time $t_i = i/30$, where i refers to the i-th day of treatment over the course of n_d days of treatment (the factor $1/30$ in t_i accounts for the fact that the unit time in the model is set to 1 month).

The differential equation for the drug concentration $I(t)$ is decoupled from the other equations in system (SE21) and can be solved with standard methods. The solution is

$$I(t) = \sum_{i=1}^{n_d} \nu e^{-\tau(t-t_i)} u(t - t_i),$$

where $u(t - t_i)$ is the unit step function. The behavior of $I(t)$ in the scale of one month is shown in Figures S9 and S10, with parameters values corresponding to pharmacokinetic properties of *imatinib* (half-life of 19 hours [3]). For *dasatinib* (half-life of 4 hours [4]), the results are similar and not shown.

In comparison with the extended model defined by equations (SE21) and (SE22), the simplified ODE model (equations (E2-E4) in the Main Text) assumes a constant, mean concentration of TKI over the time, as shown in Online Supplementary Figure S9. In order to express this mean value in terms of the pharmacokinetic parameters, we reason as follows. The description of daily doses can be approximated by a constant drug administration $v(t)$ as

$$v(t) = \nu_M,$$

where $\nu_M = 30\nu$ is the monthly TKI-dose (only considering the time range before treatment reduction or cessation). The solution for this simplified version of $v(t)$ is

$$I(t) = \frac{\nu_M}{\tau}(1 - e^{-\tau t}),$$

which quickly reaches the steady-state concentration

$$I(t) \approx I_E = \frac{\nu_M}{\tau} = \frac{30\nu}{\tau}$$

(see Online Supplementary Figure S9A). Therefore, in the simplified model, the drug concentration in the plasma is approximated by the constant mean value

$$I_E = \frac{30\nu}{\tau}.$$

Substituting this constant level in (SE21), we can disregard the equation for $I(t)$, and the new system is equivalent to our original model (first three equations in (SE21)), with the TKI-effect parameter set to

$$e_{TKI} = \frac{30k_{TKI}}{\tau}\nu.$$

From our considerations we conclude that the TKI-effect parameter e_{TKI} in our simpler model is proportional to the daily TKI-dose ν, i.e., $e_{TKI} = \kappa\nu$, where $\kappa = 30k_{TKI}/\tau$. Therefore, a dose reduction by a fraction f translates into a reduction in the TKI-effect e_{TKI} by the same fraction.

As can be seen in Online Supplementary Figure S9B and D, there is no visible difference between the solutions of the simpler model (assuming a constant mean level of TKI in the plasma) in comparison with the detailed model (explicitly considering the pharmacokinetics of TKI). On the contrary, the same behavior is observed for the decay of LSC population, thereby ensuring us that the simpler model is sufficient for deriving clinical predictions.

S11 Threshold for inhibitory concentrations of TKI

TKI plasma concentrations need a to reach a minimal threshold for effective inhibitory activity [5]. With 400mg once-daily administration, *imatinib* plasma concentration reaches a value of 2.6 +/- 0.8 microg/mL at peak level and 1.2 +/- 0.8 microg/mL at trough level, exceeding the threshold of 0.5 microg/mL for in vitro inhibition [5]. We can include this pharmacokinetic consideration in our ODE model by noting that this threshold corresponds to 19.2% of the peak

concentration. Therefore, we conclude that the TKI effect e_{TKI} depends on the TKI abundance, encompassing such threshold I_{min}. We assume

$$\hat{e}_{TKI}(I(t)) = \begin{cases} e_{TKI}, & \text{if } I(t) > I_{min} \\ 0, & \text{if } I(t) < I_{min} \end{cases} .$$

With this additional assumption, the simulation results for *imatinib* are also indistinguishably from the simplified model when the dose stays above 28.8% of the original dose. This approximate threshold indicates a substantial range for potential dose reductions, although we note that the above numbers for TKI peak and threshold concentrations are obtained from *in vitro* experiments and might require further verification. However, this estimate supports the notion that half-dose reductions appear within the safe regimen for which we do not expect sub-inhibitory TKI concentrations. However, more studies are needed to estimate the precise pharmacological limit, which may also vary between different patients.

S12 Analysis of emergence of resistance

In this section, we quantify the probability of generating resistance mutations due to increased proliferation in the reduced dose scenarios compared to the standard dose scenario. We assume that this probability is proportional to the accumulated number of LSCs division over time.

The number of LSCs divisions between times t_0 and t_F is described by the integral of the proliferation term $p_Y Y(t)$ over time, i.e.,

$$LSC_D(t_0, t_F) = \int_{t_0}^{t_F} p_Y Y(t) dt.$$

Therefore, the probability of generating a resistance mutation between times t_0 and t_F, denoted by $P_R(t_0, t_F)$, is proportional to $LSC_D(t_0, t_F)$. For the median parameters in the untreated growth phase ($e_{TKI} = 0$, no treatment; initial conditions $X(0) = 1, Y(0) = 0, W(0) = 0$), the latency time is $T = 6.45$ years to reach the median diagnosis level $L_0 = 100\%$. During this period, the number of LSC divisions adds to $LSC_D(0, T) = 1.00401 \times 10^6$. In the *treatment scenario* ($e_{TKI} > 0$, initial conditions at $t = 0$ corresponding to $L_0 = 100\%$), the number of LSCs divisions after 6 years under standard therapy is $LSC_D(0, 72m) = 169901$ divisions, while most of these divisions (98.4%) occur within the first six months of treatment when the leukemic burden is still large. These results also indicate that the number of LSC division during a 6 year treatment period accounts for only 14.5% of all LSCs divisions occurring since leukemia initiation (for the median patient within our cohort).

Now, we calculate the number of additional LSC divisions resulting from a reduced dose applied after initially treating with the standard therapy for the first 3 years. Online Supplementary Figure S10 indicates an additional 492 divisions for the $f = 50\%$ reduction (1442 divisions for the $f = 25\%$ reduction). This increase accounts for only 0.29% ($f = 50\%$) and 0.85% ($f = 25\%$), respectively, during a 6 year treatment scenario. The proportion is even more marginal (0.04% ($f = 50\%$) and 0.12% ($f = 25\%$)) if the complete leukemic episode is considered.

S13 Alternative model formulation without LSCs deactivation

The estimated individual values of the LSC deactivation rate p_{YX} are very low for almost all patients (Figure 1B) and therefore, could potentially be zero. Considering this particular case, we can define an alternative model in which we set $p_{YX} = 0$. In this alternative formulation, we introduce a parameter for the initial number of quiescent LSCs $X(0) = X_0$, since in the original model this condition is $X(0) = (p_{YX}/p_{XY})Y_0$. Following the same approach as in Online Supplementary Text S2, we obtain a different analytical correspondence between the biphasic and the mechanistic model parameters. In this alternative scenario, the formulas for α and β read (instead of formulas (SE5)):

$$\alpha = -q, \;\; \beta = -p_{XY}.$$

These exact solutions of the alternative model are identical to the approximate solutions of the model considering stem cell deactivation. Thus, the interpretation that the second decline is limited by the activation of quiescent LSCs is still valid. Although the model might appear simpler, the statistical approach for model fitting remains the same, because we first find the values of the phenomenological parameters A, B, α, β and then use these values to calculate the model parameters L_0, q, p_{XY} and p_{YX} (or X_0 in this alternative model). Therefore, the interpretation of the slopes is identical to our approximate solution with the original model, and we can conclude that the same results for dose reduction are expected for this alternative model formulation.

References

[1] F. Michor, T. P. Hughes, Y. Iwasa, S. Branford, N. P. Shah, C. L. Sawyers, and M. A. Nowak, "Dynamics of chronic myeloid leukaemia", *Nature*, vol. 435, no. 7046, p. 1267, 2005.

[2] I. Roeder, M. Horn, I. Glauche, A. Hochhaus, M. C. Mueller, and M. Loeffler, "Dynamic modeling of imatinib-treated chronic myeloid leukemia: Functional insights and clinical implications", *Nature medicine*, vol. 12, no. 10, p. 1181, 2006.

[3] C. Kogel and J. Schellens, "Imatinib.", *The oncologist*, vol. 12, no. 12, pp. 1390–1394, 2007.

[4] A. Hochhaus and H. Kantarjian, "The development of dasatinib as a treatment for chronic myeloid leukemia (cml): From initial studies to application in newly diagnosed patients", *Journal of cancer research and clinical oncology*, vol. 139, no. 12, pp. 1971–1984, 2013.

[5] B. Peng, P. Lloyd, and H. Schran, "Clinical pharmacokinetics of imatinib", *Clinical pharmacokinetics*, vol. 44, no. 9, pp. 879–894, 2005.

	Initial	Filter 1 ("data" criteria)	Filter 2 ("data" criteria)	Filter 3 ("data" criteria)	Filter 4 ("data" criteria)	Filter 5 (DESTINY criteria)	Filter 6 (DESTINY criteria)	Final	Classification (% relative to "Final")	
Study	Initial number of patients	less than 5 data-points	$\beta > 0$	$\beta < \alpha < 0$	any *BCR-ABL1* ratio >500%	under TKI for less 36m	no MR3 in the last 12m	selected patients	MR3 cohort	MR4 cohort
IRIS	69 (100%)	3 (4%)	9 (13%)	1 (1%)	1 (1%)	4 (6%)	4 (6%)	47 (68%)	35 (75%)	12 (25%)
CML-IV	280* (100%)	70 (25%)	71 (25%)	3 (1%)	1 (0%)	49 (18%)	10 (4%)	75 (27%)	25 (33%)	50 (67%)

Online Supplementary Table S1. Filter criteria for the patient cohort.
For the quantitative analysis we selected patient time courses according to the following criteria: (Filter 1) excluding patients with less than 5 *BCR-ABL1* measurements at different time points, which are insufficient for the fitting routine for the bi-exponential decline; (Filter 2) excluding patients with a bi-exponential fit $\beta > 0$, corresponding to patients with increasing *BCR-ABL1* levels; (Filter 3) excluding patients with monophasic or inverted biphasic decline ($\beta < \alpha < 0$); (Filter 4) excluding patients with any *BCR-ABL1* measurements above 500%, indicating a pronounced non-linearity between *BCR-ABL1* abundance and tumor load. For comparison with the DESTINY cohort, we further excluded (Filter 5) patients treated with TKI for less than 36 months and (Filter 6) patients which were not below MR3 in the entire last year of follow-up. *) From the 280 available patients, one could not be evaluated as no reasonable BCR-ABL1 levels values were reported.

% of patients predicted to retain long-term treatment efficiency after de-escalation by 50% (results in main text and supplementary figure S8A)			% of patients predicted to loose MR3 within 1 year after dose de-escalation by 50% (results in figure 4A)						
	IRIS	CML-IV		IRIS	IRIS MR3 cohort	IRIS MR4 cohort	CML-IV	CML-IV MR3 cohort	CML-IV MR4 cohort
original data	90%	81%	**original data**	5.4%	7.3%	0.25%	2.8%	8.3%	0.25%
modified data for high BCR-ABL1 levels	90%	79%	**modified data**	5.3%	7.1%	0.25%	2.6%	8.0%	0.25%

Online Supplementary Table S2. Robustness of model results with respect to the reliability of high *BCR-ABL1* values.
We tested the robustness of our main quantitative conclusions with respect to the handling of high *BCR-ABL1* values. As such, we reran all selection steps, empirical data fitting and model simulations under the limitation that all *BCR-ABL1* values *above* 100% in the primary data are set to strictly 100%. The numerical analysis of the resulting $n = 127$ patients ($n = 48$ in IRIS and $n = 79$ in CML-IV; different numbers result from minor changes in filter steps 2 to 4, Online Supplementary Table S1) revealed qualitatively and quantitatively similar results compared to the less restrictive, original setting. This indicates a good robustness of our overall conclusions with respect to the reliability of high *BCR-ABL1* values.

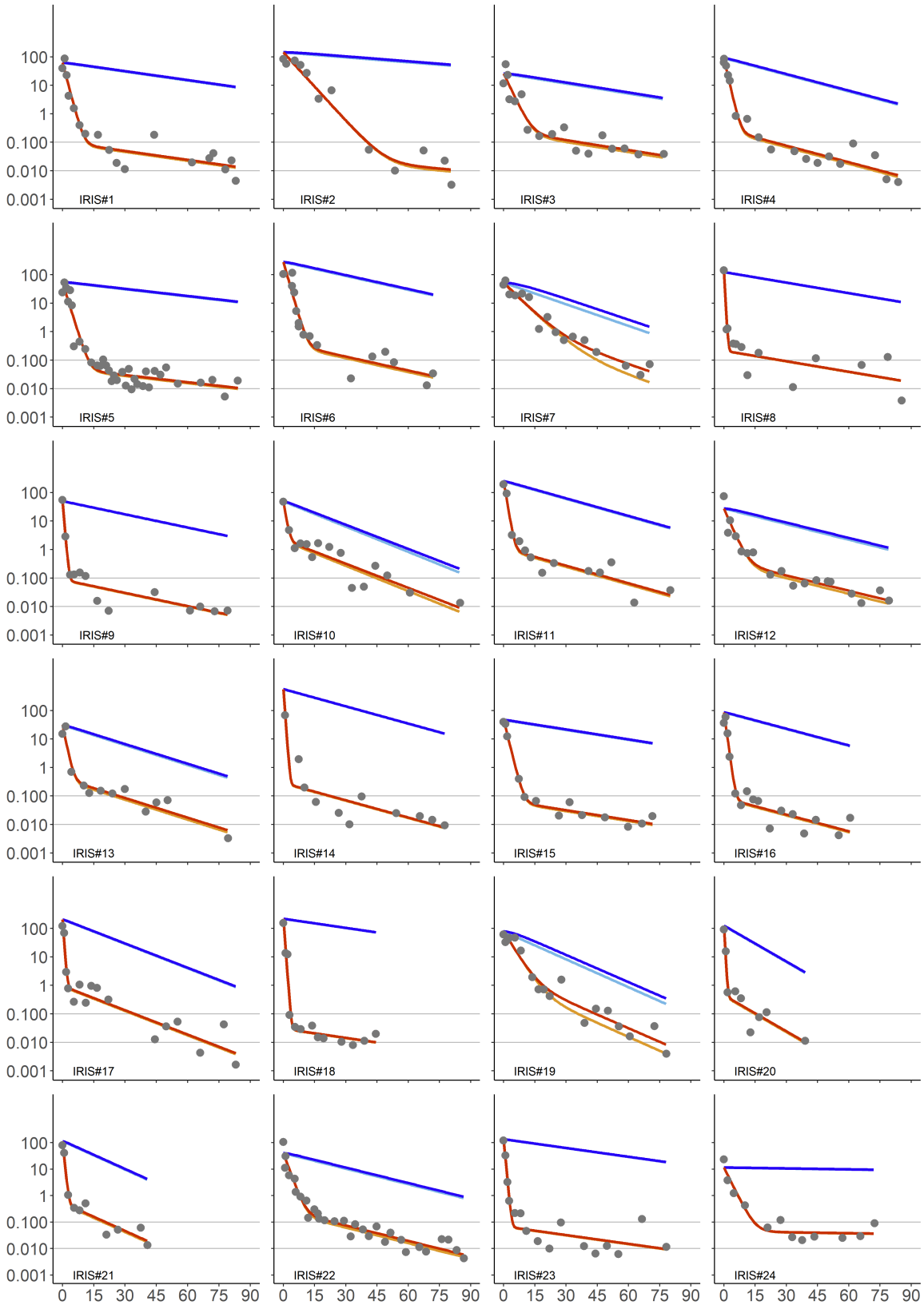

Online Supplementary Figure S1. Individual patient *BCR-ABL1* data and model exact and approximated solutions. Individual treatment data (dots, triangles for undetectable values), i.e., *BCR-ABL1* ratios, of each patient within the IRIS and CML-IV cohorts, the corresponding bi-exponential fit, and the model's exact solution (red). From the calculated individual parameters, we predict the *BCR-ABL1* levels of quiescent LSCs (blue) and model approximations for the *BCR-ABL1* levels of proliferating (orange) and quiescent (light blue) LSCs; compare equations SE8 and SE10 in Supplementary Text.

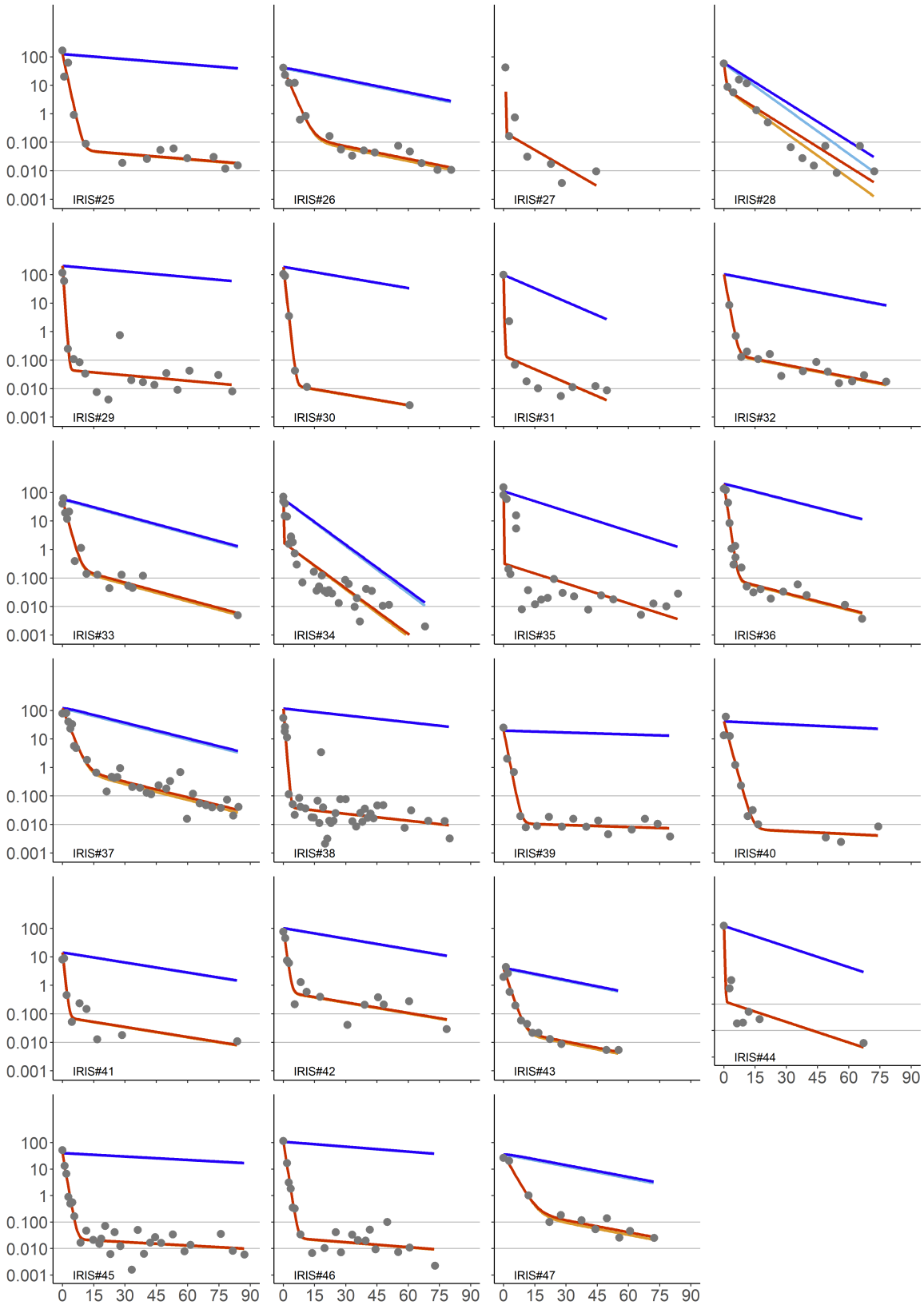

Online Supplementary Figure S1 continued

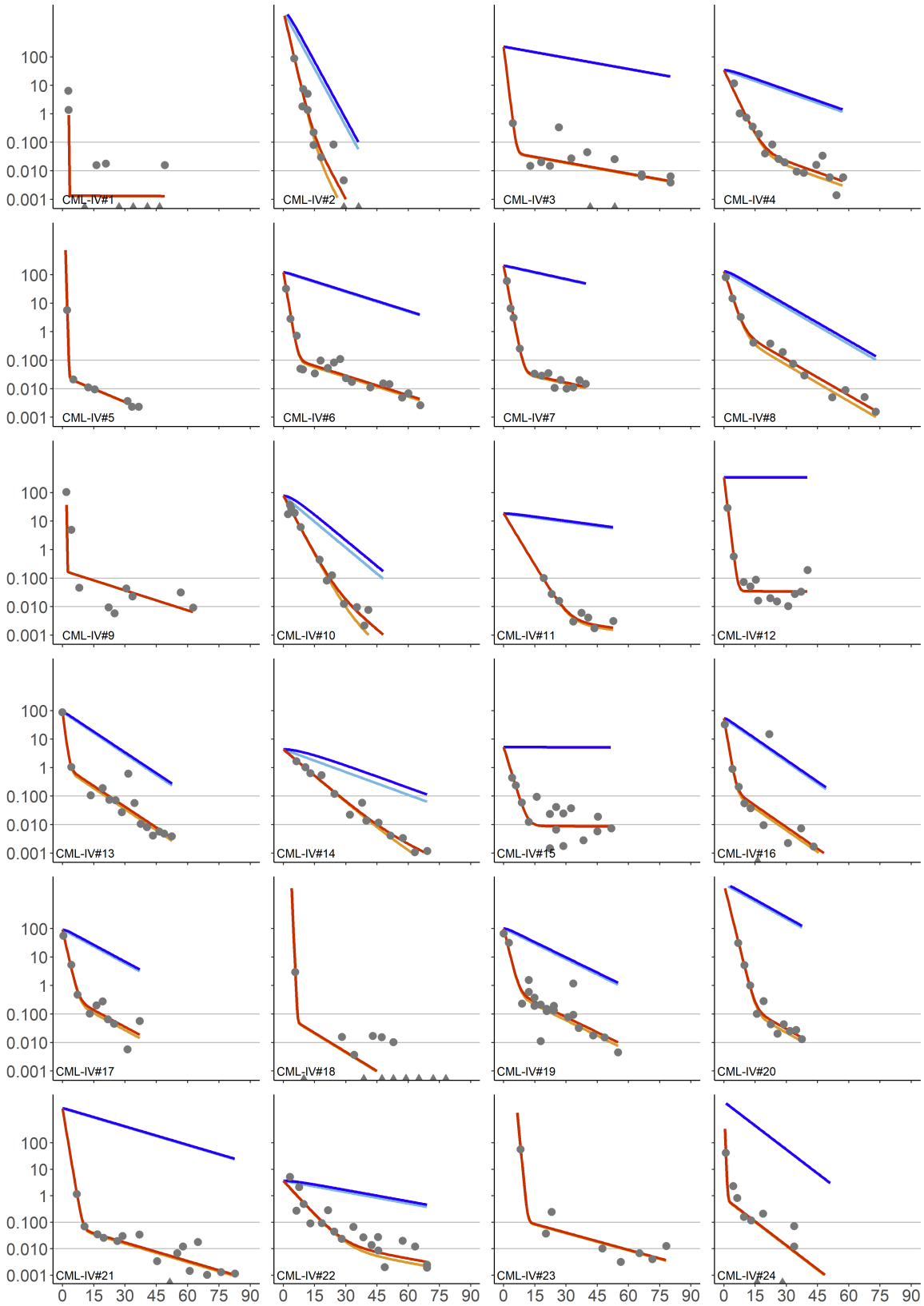

Online Supplementary Figure S1 continued

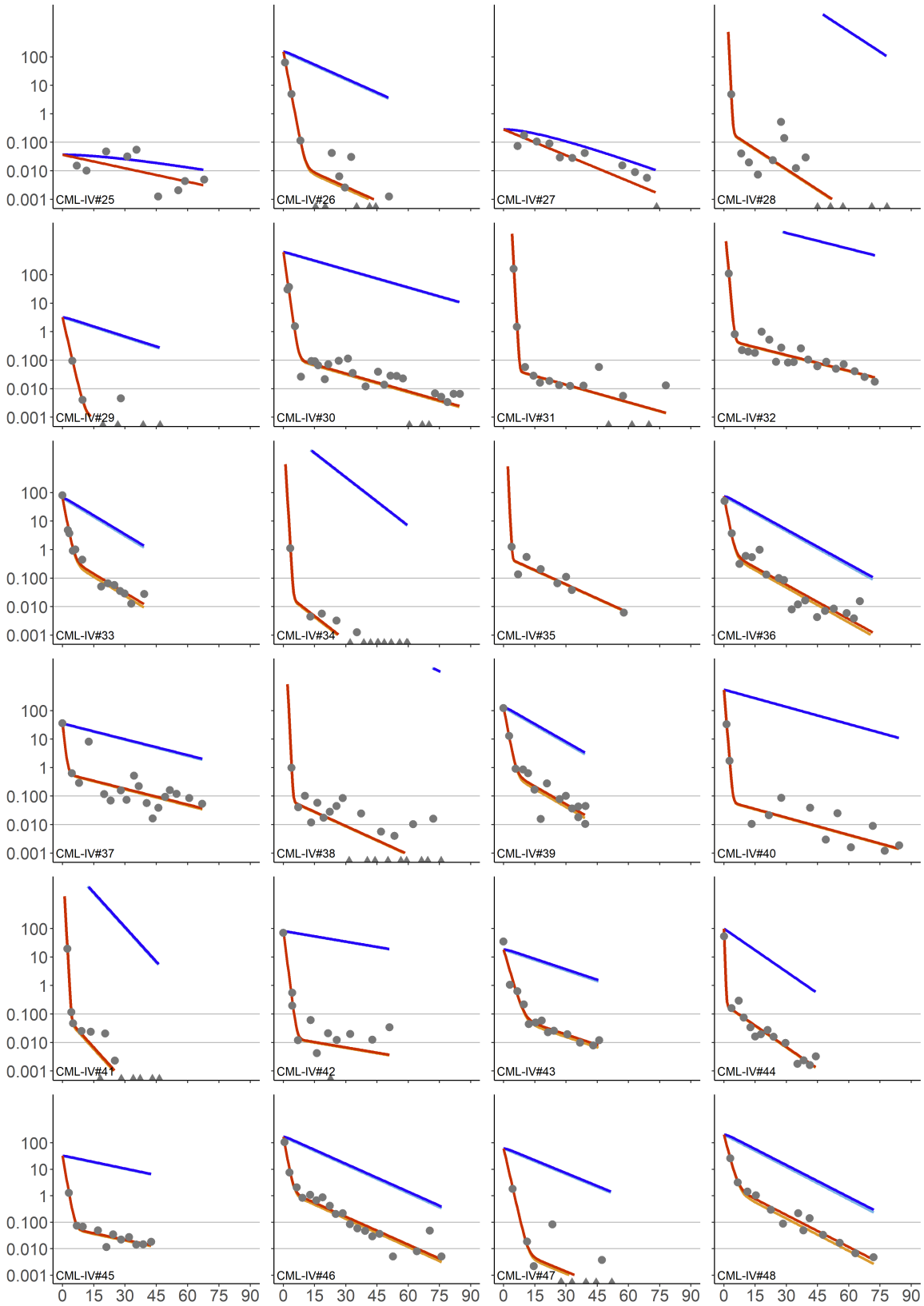

Online Supplementary Figure S1 continued

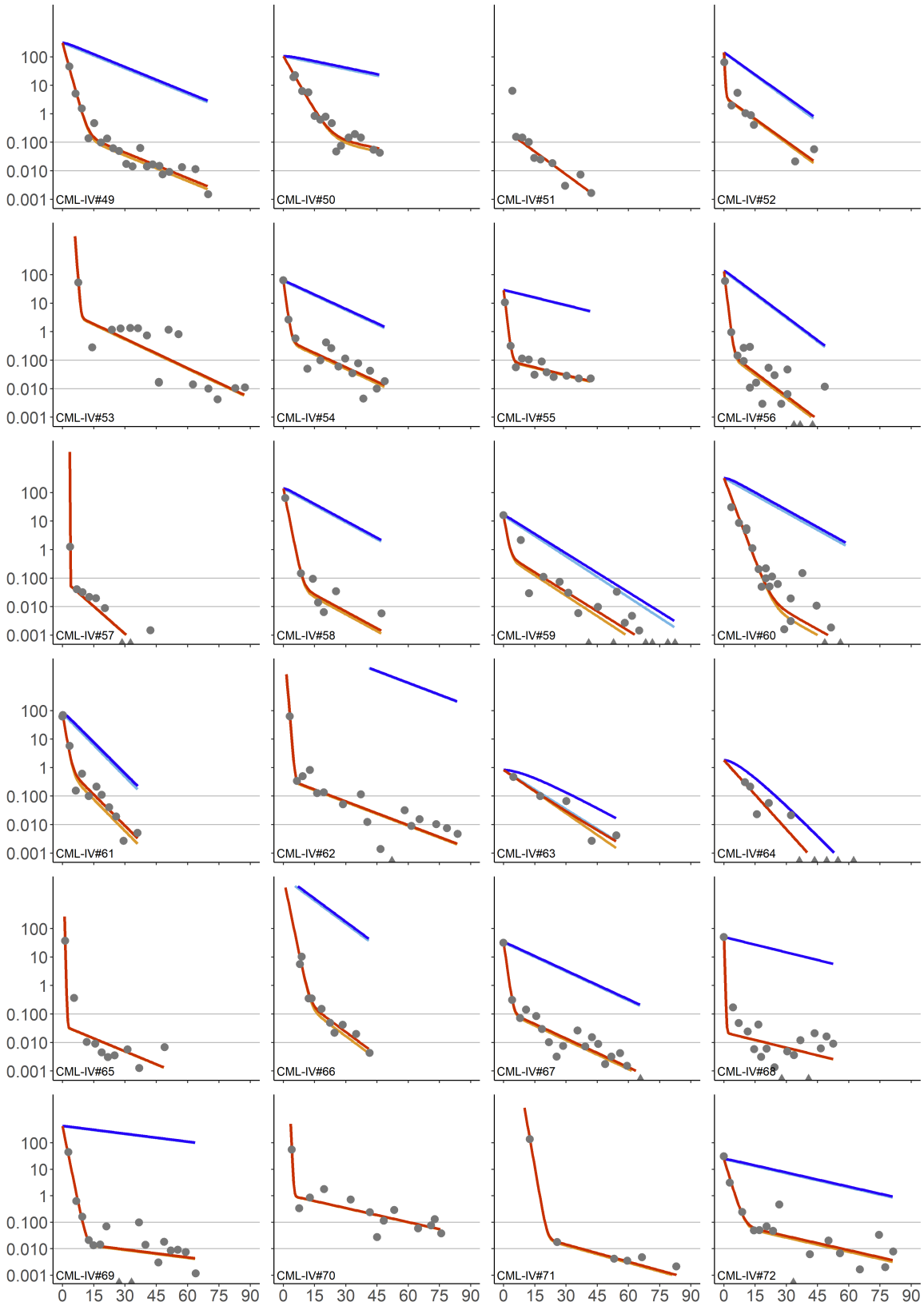

Online Supplementary Figure S1 continued

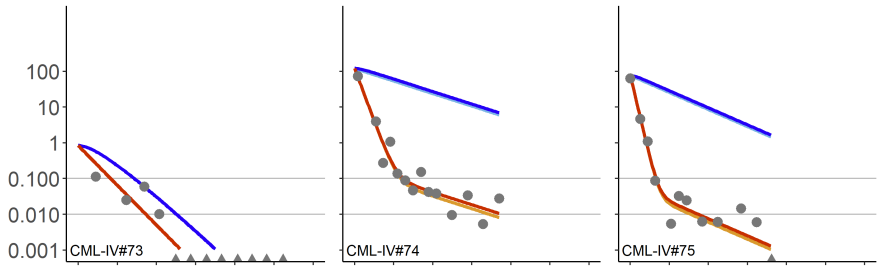

Online Supplementary Figure S1 continued

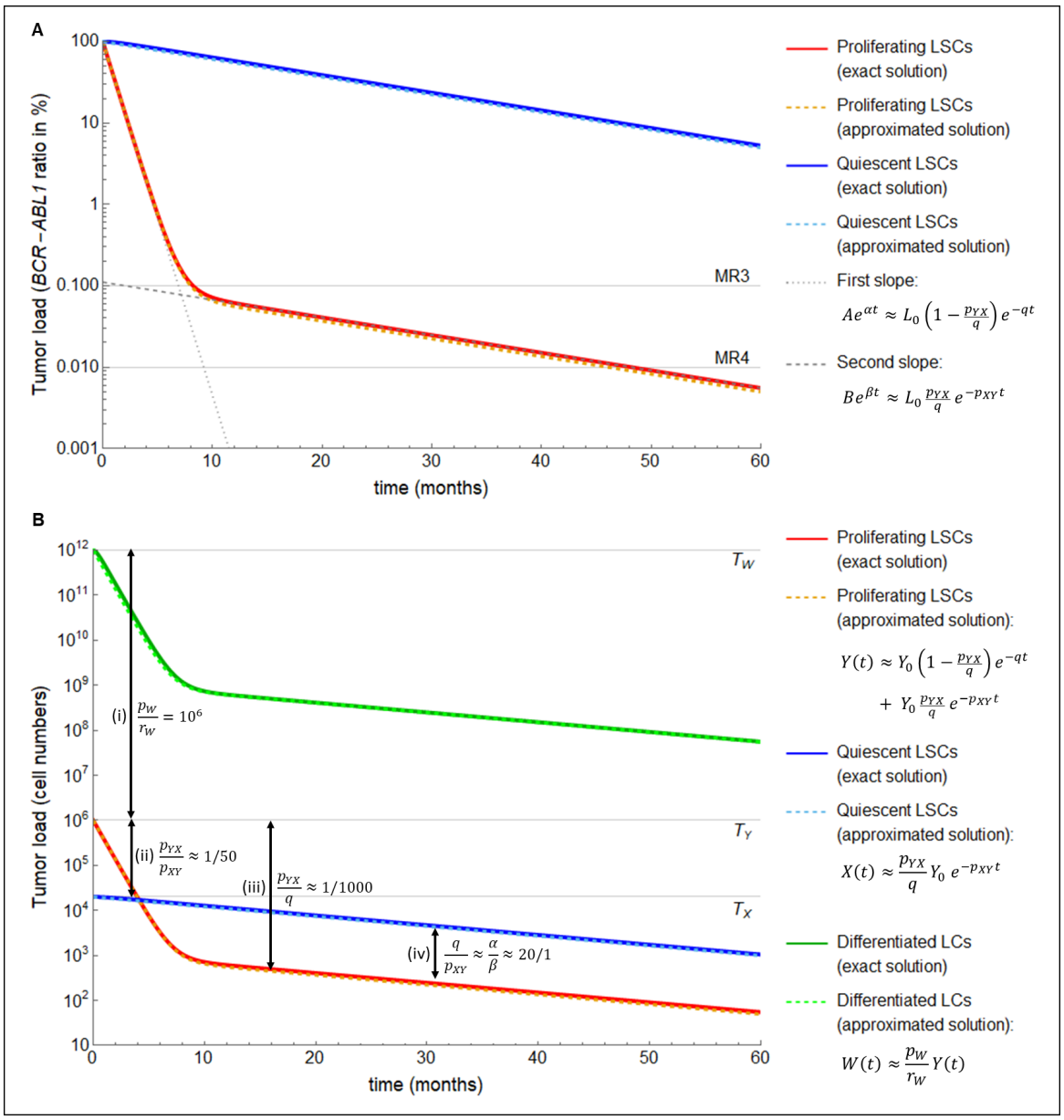

Online Supplementary Figure S2. Comparison of exact and approximated solutions for relative and absolute cell numbers.

Solid lines indicate exact solutions; dashed lines represent approximated solutions after accounting for the intrinsic scaling between model parameters (equations (SE7,8,9,10) in Online Supplementary Text S6). Simulations are based on approximated median parameter values of available IRIS and CML-IV patients (see Online Supplementary Figure S1 and Online Supplementary Table S1). **A)** Exact and approximated solutions in terms of *BCR-ABL1* levels. The close correspondence indicates that focusing on the dominating treatment effects (the effective TKI effect $q = e_{TKI} - p_Y$ during the initial slope and the rate p_{XY} during the second slope) is fully sufficient to reflect the overall treatment dynamics. The approximations also reveal that quiescent LSCs follow a monophasic decline with slope β during the entire treatment, and that the fraction of proliferating LSCs that remain after the first decline is approximately p_{YX}/q. **B)** Assessing the model dynamics in terms of absolute cell numbers reveals an identical correspondence between exact and approximated solutions. Furthermore, we highlight: (i) For each proliferating LSC, there are $p_W/r_W = 10^6$ differentiated LCs; this proportion remains constant during the entire treatment. (ii) The initial number of quiescent LSCs at treatment start is a ratio p_{YX}/p_{XY} of the number of proliferating LSCs, corresponding to approximately 1 quiescent for every 50 proliferative LSCs. (iii) The fraction of proliferating LSCs that remain after the first slope is p_{YX}/q, i.e. 0.1% of the original population, indicating a reduction of 3 log-scales corresponding to a major molecular remission (MMR, MR3). (iv) After the massive reduction in the abundance of proliferating LSCs, the proportion of quiescent/proliferative LSCs is inverted, and the number of proliferative LSCs only accounts for a small fraction of the total LSC population. The ratio X/Y is approximated both by q/p_{XY} and α/β (see Online Supplementary Text S7), corresponding to approximately 20 quiescent LSCs for each proliferative LSC, and remaining constant over the time.

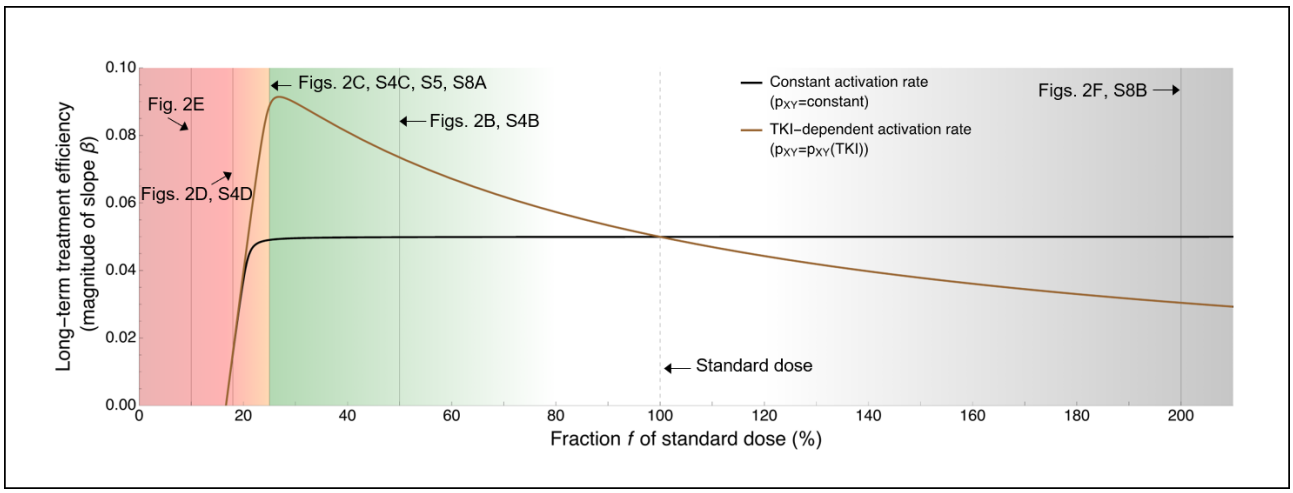

Online Supplementary Figure S3. The long-term treatment efficiency as a function of the TKI dose.
The long-term treatment efficiency (defined as the magnitude of slope β), plotted as a function of the TKI dose (black line), is constant in a large interval encompassing both lower and higher doses as compared to the standard dose. See Figure 2 and Online Supplementary Figures S4, S5 and S6 for model simulations of dose modifications corresponding to the marked (vertical lines). Assuming an additional TKI-effect on the activation rate p_{XY} leads to an alternative scenario (brown line). In this case, the benefit of dose de-escalation is even better, while an impairment in the long-term efficiency is expected for higher dose. A dose de-escalation decreases the inhibitory effects of TKI on quiescent cell activation, thereby allowing more of these cells to become proliferating and then be targeted by TKI.

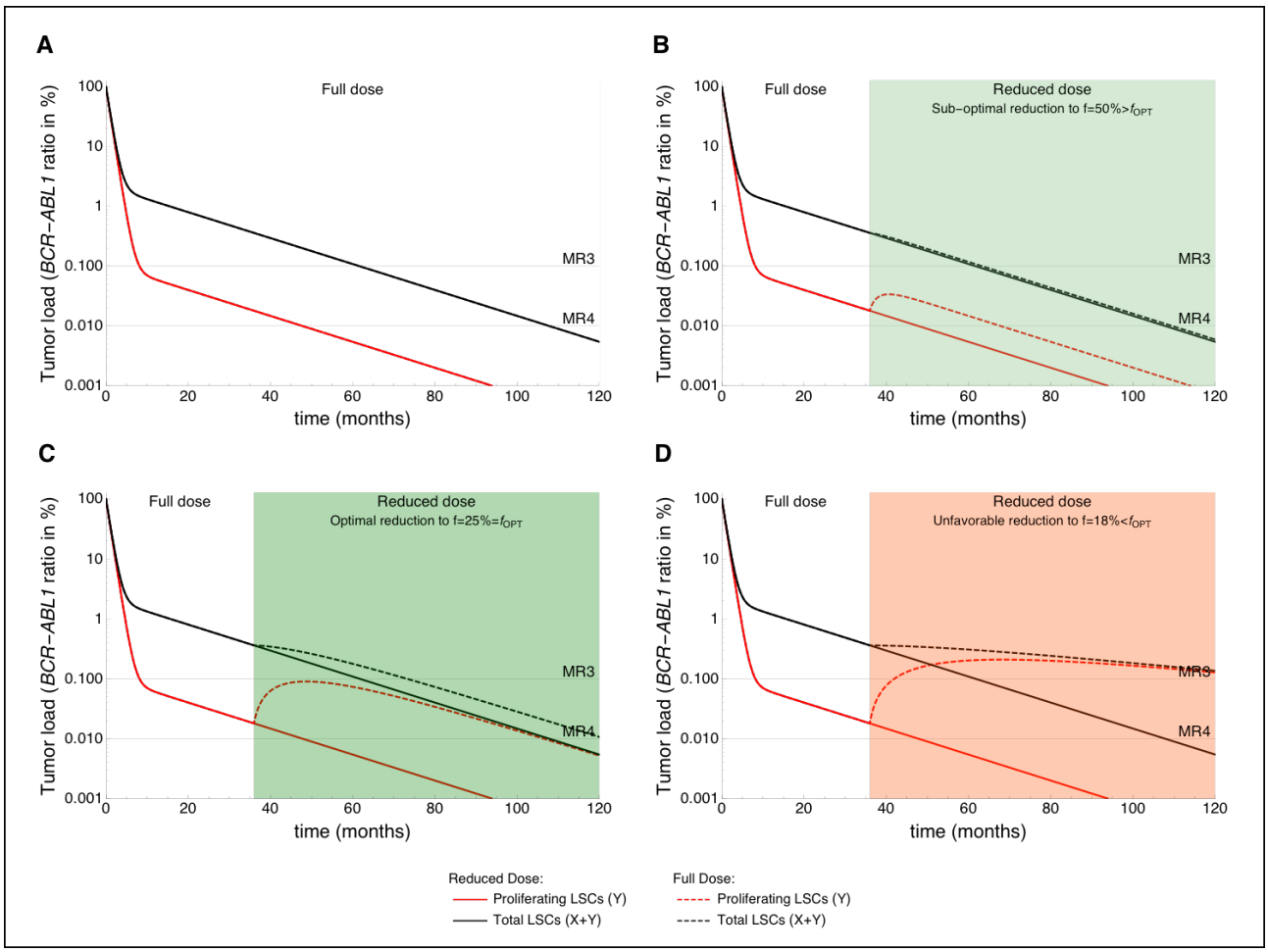

Online Supplementary Figure S4. Response of total LSCs to full and reduced dose. Dynamics of all LSCs (proliferating + quiescent; black) and of proliferating LSCs (red) in different dose scenarios of dose reduction. The vertical axis indicates the percentage of cells with respect to the total number of stem cells, $T_X + T_Y$ (see Methods); the black line corresponds values $(X(t)+Y(t))/(T_X+T_Y)$ while the red line corresponds to values $Y(t)/(T_X+T_Y)$.
A) Full dose scenario, corresponding to figure 1C and Online Supplementary Figure S2. At diagnosis, most of LSCs are in the proliferative state. The 3-log reduction in this compartments during the first decline implies that, during the whole long-term phase of treatment, most of the LSCs are in the quiescent state. Therefore, the long-term treatment efficiency is bounded by the activation rate of quiescent LSCs, which leads to the slower secondary decline.
B,C) Half and optimal dose scenarios, corresponding to figures 2B and 2C, respectively. The transient increase in the proliferating LSCs compartment represent a irrelevant/minor (B/C) change in the dynamics of the larger compartment comprising all LSCs. Due to the log-scale effect, the differences between the dashed (reduced dose) and continuous (full dose) lines are more prominent for lower values of the tumor load, i.e., in for the red curves.
D) Unfavorable reduction scenario, corresponding to figure 2D. The reduced dose is too low to prevent the growth of proliferating LSCs, which increase in number and then become the major part of the overall LSCs compartment.

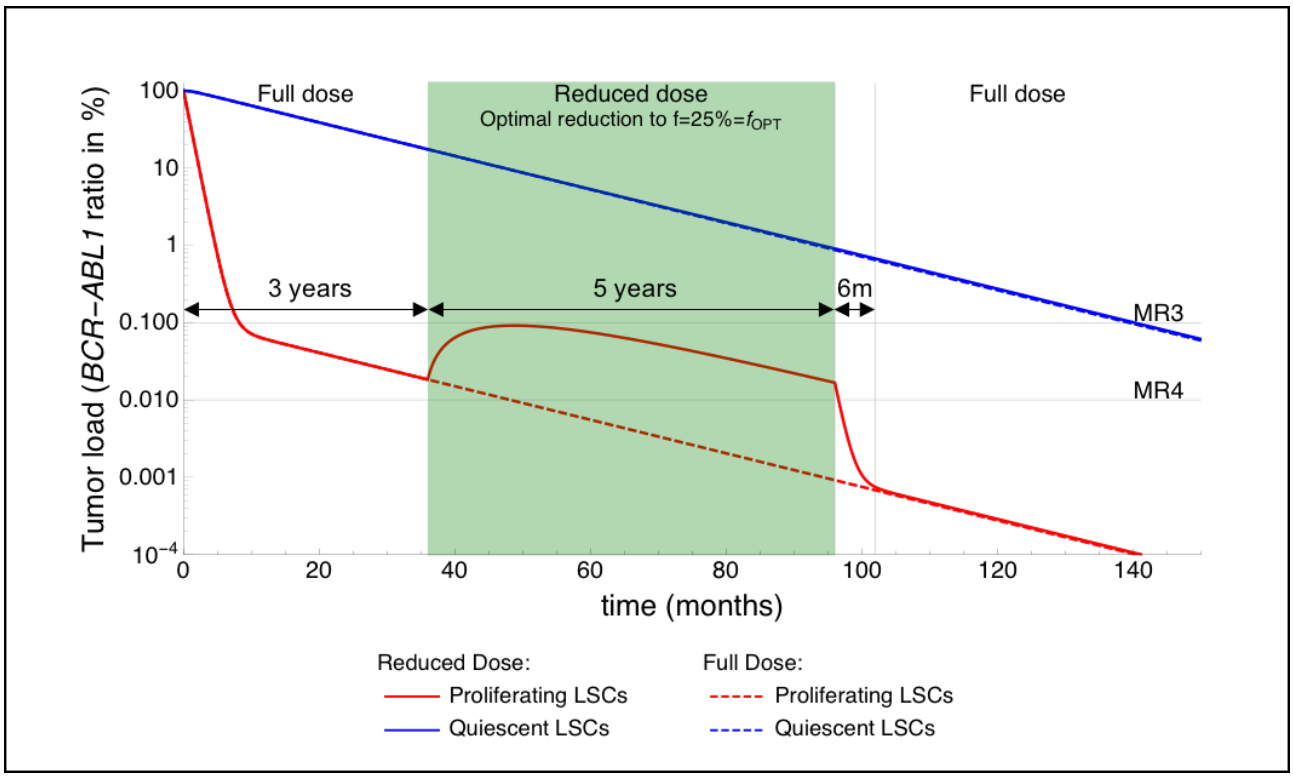

Online Supplementary Figure S5. Model prediction for resumption of full dose five years after dose de-escalation. Model simulation comprising three different treatment regimens: full dose for three years, followed by optimal dose ($f = 25\%$) for five years, followed full dose. The increased population of proliferating LSCs observed after dose de-escalation (in comparison with full dose) is reduced to the full dose levels within six months after resumption, indicating that the proliferating population of LSCs responses to dose modifications in the short-term, but then are again depleted at a rate equal to the activation rate of quiescent LSCs.

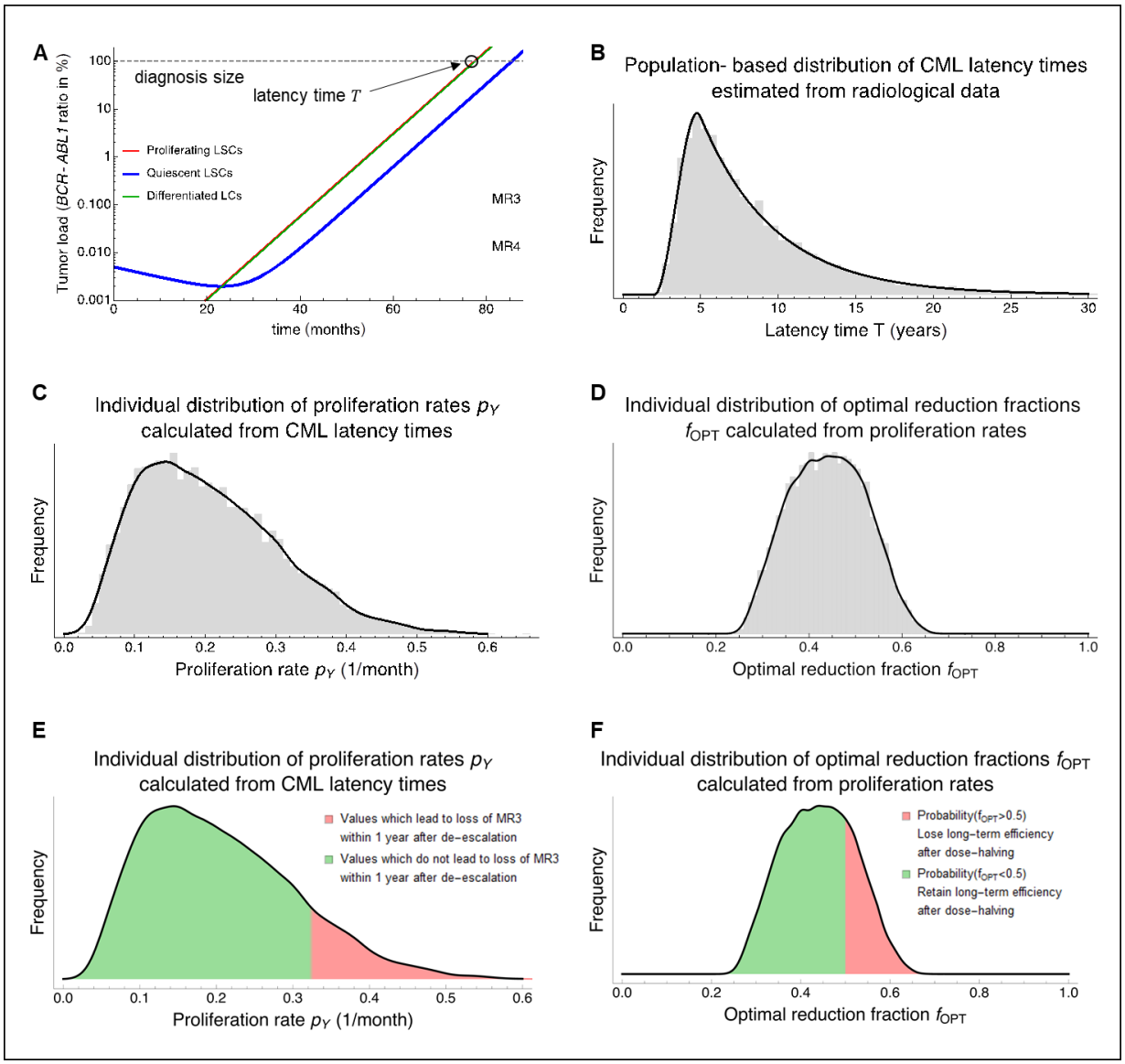

Online Supplementary Figure S6. Using CML latency times to estimate patient specific distributions of p_Y and f_{OPT}.

A) The CML latency time is defined as the time T between the emergence of the first leukemic cell and the disease diagnosis. For each patient, using the patient specific parameters p_{XY}, p_{YX}, q and L_0, and assuming a particular value of p_Y, the latency time can be calculated by simulating equations (E2-E4) with $e_{TKI} = 0$ and initial conditions $X(0) = 1$, $Y(0) = X(0) = 0$ to determine the time T needed to reach an estimate of the tumor load at diagnosis (approximated by the first *BCR-ABL1* measurement, L_0). The inverse problem can also be solved, i.e., given a certain value of the latency time T, it is possible to find the value of p_Y such that the model predicts the given latency time. Using this approach, we obtained patient specific distributions for p_Y and f_{OPT} as follows.

B) Sampling of $N = 10,000$ values of T according to the population-based distribution of CML latency times derived by [Radivoyevitch, T., et al., Blood, 2012]. The obtained values are then assumed to be the possible latency times T observed within the patient-cohort.

C, D) For each patient, using the individual patient parameters q, p_{XY}, p_{YX} and L_0, and the steps described in (A), we calculated, for each value of the sampled latency times T, the corresponding value of p_Y. The union of all these values results in the expected individual distributions of p_Y (C), reflecting a spectrum for the possible aggressiveness of the initial leukemia. Then, for each of these values, we calculated (using equation (E6)) the corresponding values of f_{OPT}, resulting in a patient-individual distribution of values indicating the optimal dose reduction given a particular aggressiveness of the leukemia (D).

E) From the estimated, patient-specific distribution of p_Y, we calculated the fraction of values of p_Y, which lead to loss of MR3 within 1 year after de-escalation by 50%. This can be used as an estimate for the individual probability of loss of MR3.

F) From the estimated, patient-specific distribution of f_{OPT}, we calculated the fraction of values of f_{OPT} below 0.5, which can be used as an estimate for the individual probability of retaining the long-term treatment after de-escalation by 50%.

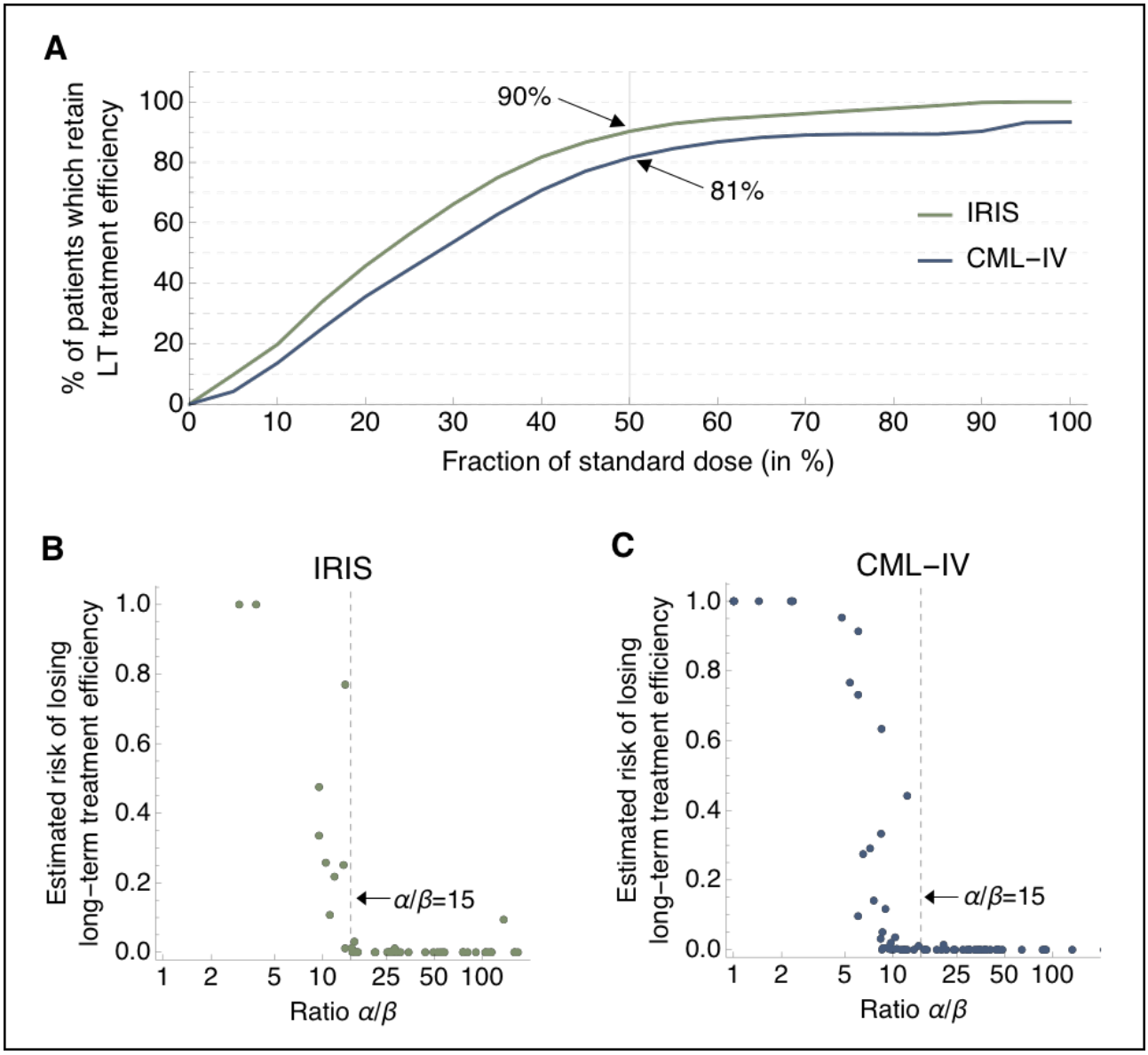

Online Supplementary Figure S7. Predicted effect of dose reduction on long-term treatment efficiency.
For the shown simulation results, we assumed a population-based distribution of CML latency as described in [Radivoyevitch, T., et al., Blood, 2012]. **A)** The predicted percentage of patients which retain the long-term treatment efficiency after a dose de-escalation to a fraction of the original dose is plotted as a function of the simulated reduced dose. For a reduction by half (vertical line at 50%), the expected percentages are 90% and 81% for the IRIS and CML-IV data-sets, respectively. **B,C)** Each dot represents an individual patient within the cohort of 122 selected patients ($n = 47$ in IRIS, green dots; $n = 75$ in CML-IV, blue dots). For each patient we determined the risk of losing the long-term efficiency after halving the dose (i.e. the probability that a 50% dose reduction leads to a less steep β slope than the standard dose) and compared with their individual α/β slope ratio. The results predict that patients with slopes satisfying $\alpha/\beta > 15$ have a very low risk to lose long-term treatment efficiency under a 50% dose de-escalation.

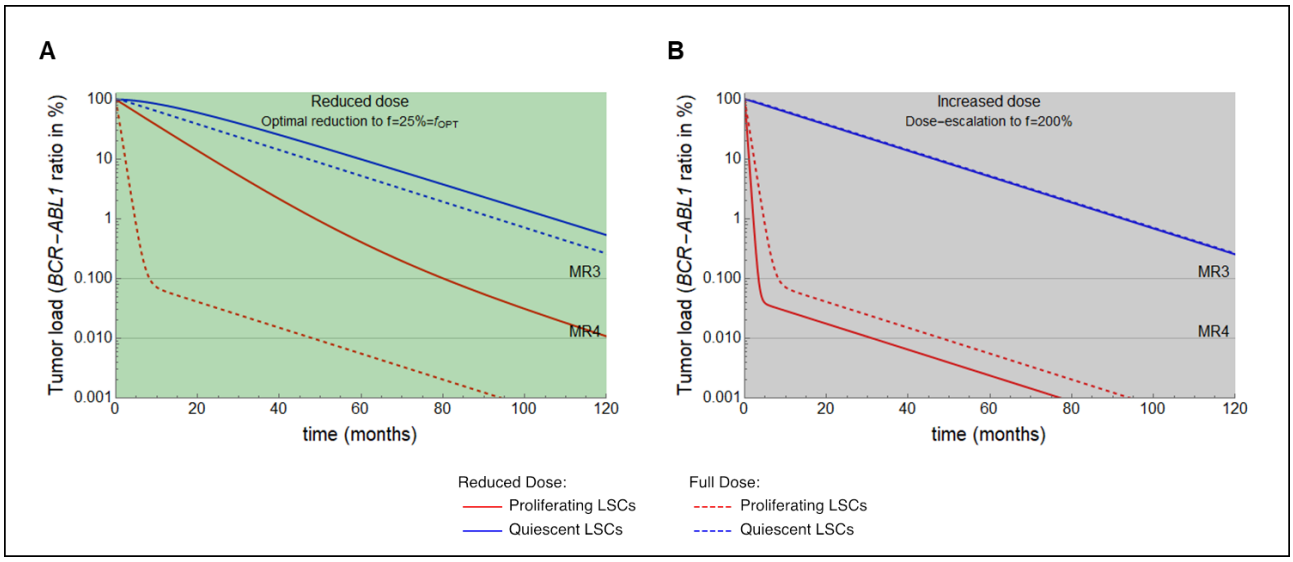

Online Supplementary Figure S8. Scenarios of dose modification.
Model simulations starting with modified doses (continuous lines) in comparison with standard dose (dashed lines). **A)** the treatment starts with the optimal dose $f = f_{OPT}$; in this case, the slopes satisfy the relation $\alpha/\beta \approx 2$, which suggests a criterion to classify patients according to their initial response, as either being "over-treated" ($\alpha/\beta \gg 2$, which would benefit from dose de-escalation) or "under-treated" ($\alpha/\beta < 2$ or monophasic declines $\alpha/ \approx \beta$, which would benefit from higher doses). **B)** treatment starting with escalated dose to $f = 200\%$; the initial response is faster and deeper in comparison with the standard dose, which agrees with results from the RIGHT trial [Cortes, J.E., et al., J Clin Oncol, 2009], which assessed the benefits of 800mg daily Imatinib in CML patients. However, the long-term treatment efficiency is predicted to be the same as in standard dose.

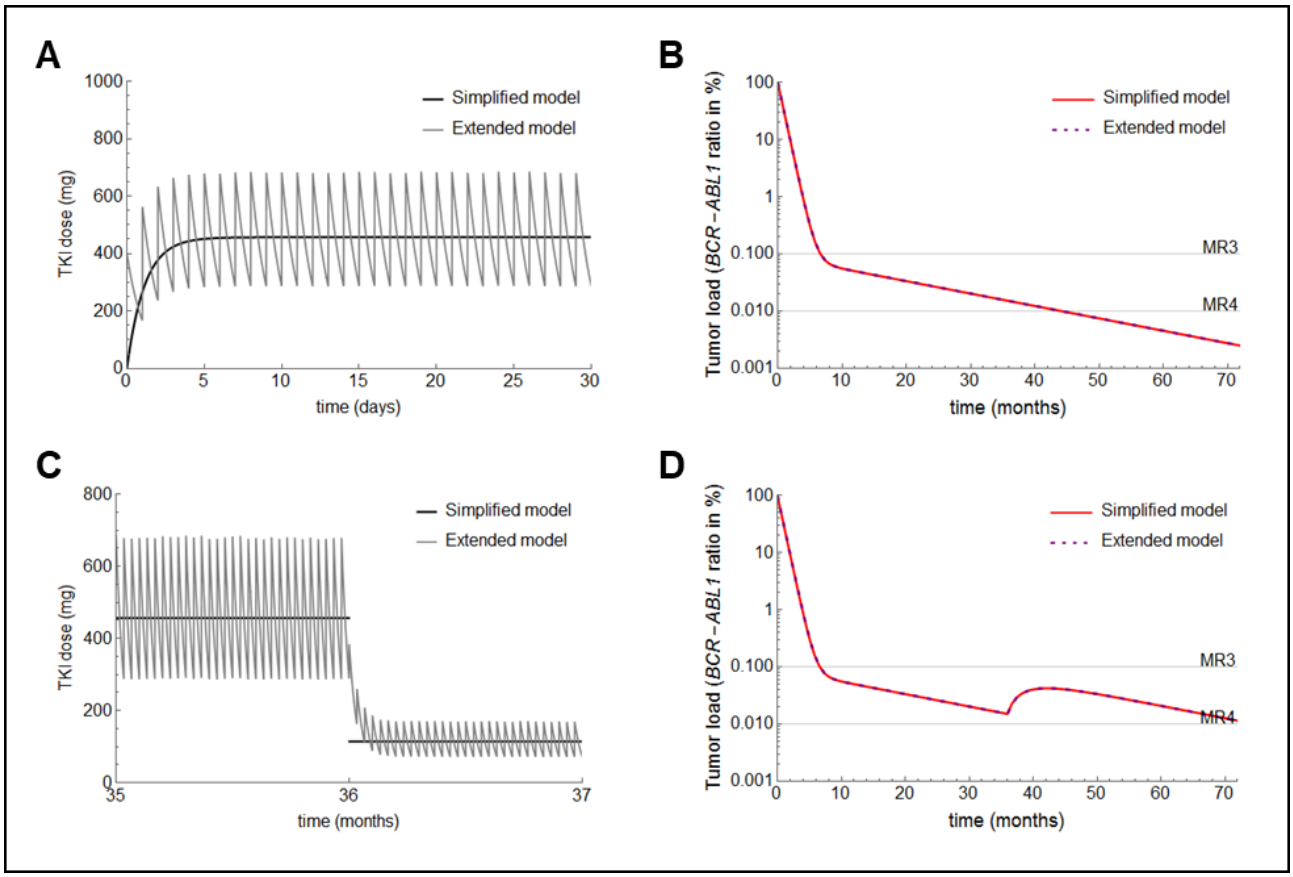

Online Supplementary Figure S9. Simulation results of an extended model explicitly considering TKI pharmacokinetics.
A,C) Simulation results showing the TKI concentration in different time intervals (A - first month of treatment, C - two months around dose reduction to $f = 25\%$) , using an extended model which explicitly considers the pharmacokinetics of daily drug intake (gray line). The simplified model assumes a constant, mean value for the TKI concentration, corresponding to continuous drug administration. **B,D)** Simulation results of the original and the extended model, showing the evolution of tumor load under standard (B) and reduced dose (D) treatment scenarios. There is no visible difference in the solution when using the different models, indicating that the simplified model represents a suitable approximation of the more detailed, pharmacokinetic approach.

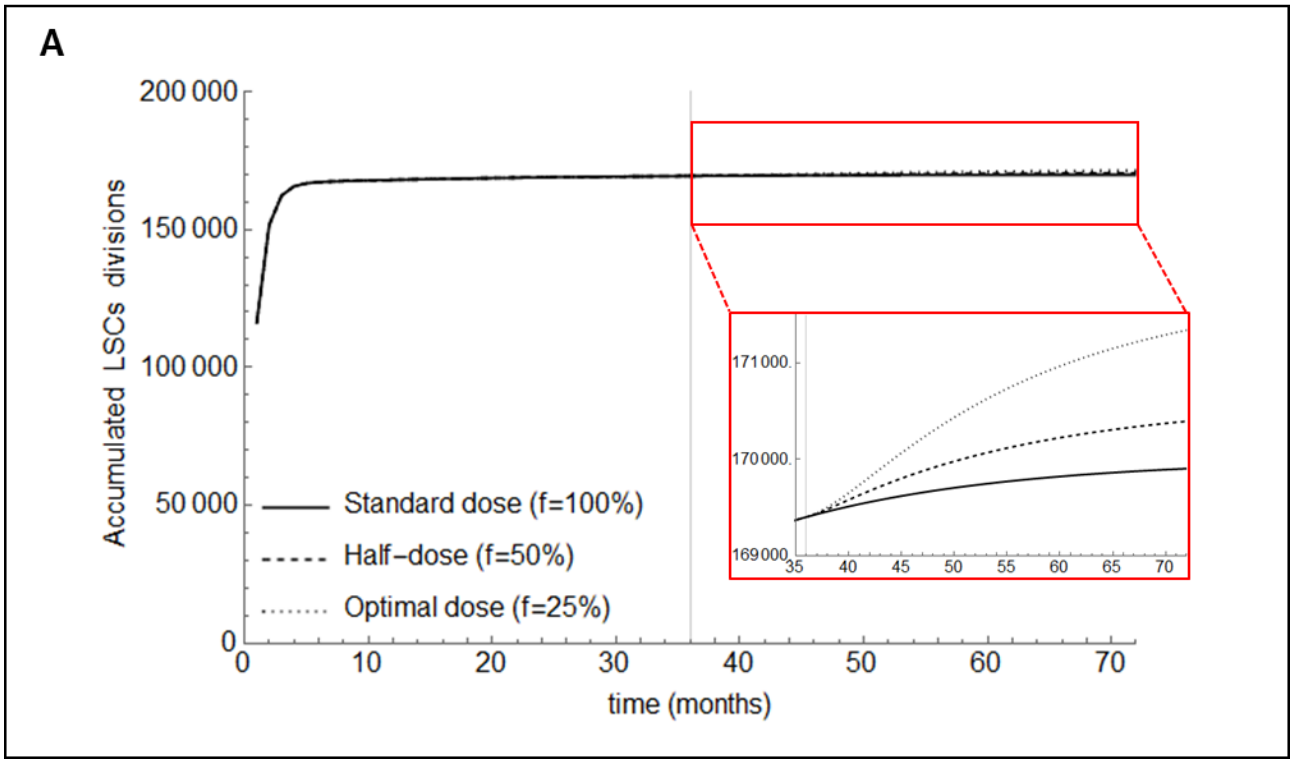

Online Supplementary Figure S10. Accumulated number of LSCs divisions over time.
Simulation results showing the accumulated number of LSCs divisions after treatment initiation, considering different dose reduction scenarios. During the first three years, the simulations assume that all scenarios use the same standard dose. After this period, the number of LSCs divisions is marginally increased in the reduced doses scenarios.

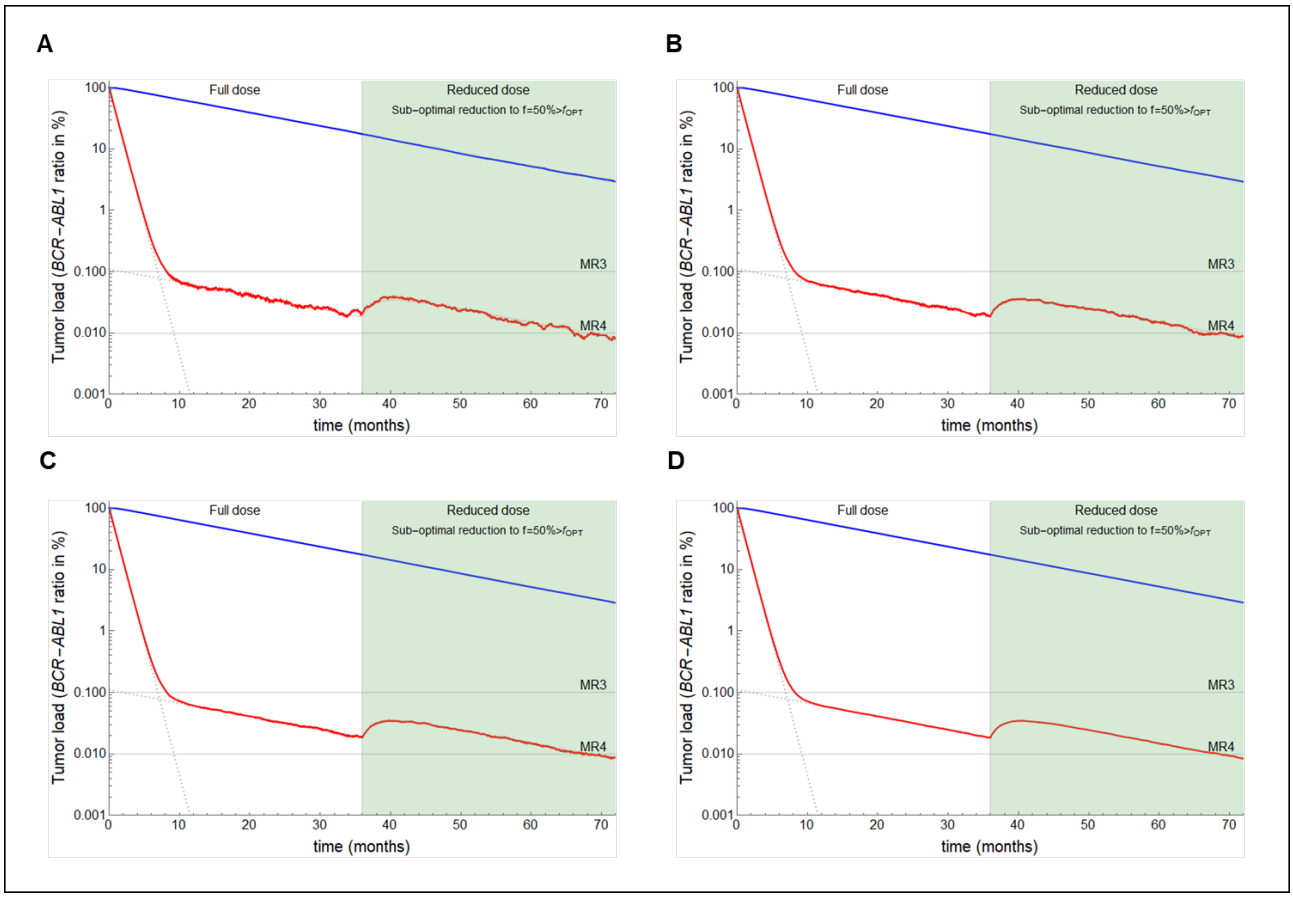

Online Supplementary Figure S11. Stochastic model simulations using a Gillespie algorithm.
We performed stochastic model simulations for the "mean patient" (see section 11 “Stochastic model simulations”). Subfigure **A)** shows the results of a single stochastic simulation, while the other subfigures present averages over 5 **(B)** , 10 **(C)** and 100 **(D)** independent simulations.